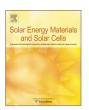
ELSEVIER

Contents lists available at ScienceDirect

Solar Energy Materials & Solar Cells

journal homepage: www.elsevier.com/locate/solmat



Defect engineering of ZnS thin films for photoelectrochemical water-splitting under visible light



Fran Kurnia a, Yun Hau Ng b, Rose Amal b, Nagarajan Valanoor a, Judy N. Hart a,*

- ^a School of Materials Science and Engineering, UNSW Australia, UNSW Sydney 2052, Australia
- b Particles and Catalysis Research Group, School of Chemical Engineering, UNSW Australia, UNSW Sydney 2052, Australia

ARTICLE INFO

Article history: Received 18 December 2015 Received in revised form 11 April 2016 Accepted 12 April 2016

Keywords: Photocatalysis Photoelectrochemistry Zinc sulfide Thin films Defects

ABSTRACT

Efficient hydrogen production from water by photocatalysis under sunlight requires a significant improvement in light-harvesting capability. Zinc sulfide is a promising, inexpensive hydrogen generation photocatalyst, but in its pure, bulk form it is only active under ultra-violet light. Here, we show clear evidence of photoelectrochemical activity of ZnS thin films under visible-light irradiation without any cocatalysts, achieved through defect engineering. Fabrication of nanostructured ZnS under controlled conditions introduces defects, and hence intermediate electronic states within the band gap, which allow significant absorption of light at energies below the band gap energy of pure, bulk ZnS. The measured band gap of the ZnS thin films is ~ 2.4 eV, while the photocurrent density exceeds 1.5 mA/cm² under visible-light irradiation ($\lambda \ge 435$ nm). This is the first measurement of such high photocurrents for undoped ZnS under visible light.

© 2016 Elsevier B.V. All rights reserved.

1. Introduction

Given the wide availability and abundance of both water and solar energy, a promising method of hydrogen production is direct photocatalytic splitting of water under sunlight [1,2]. Major limitations to achieving high photocatalytic efficiency using solar energy are restriction of light absorption to high energy (e.g. UV) wavelengths and the fast recombination of charge carriers [1,2]. In addition, expensive co-catalysts, such as platinum, are often needed to enhance charge separation and surface reaction kinetics [3].

Zinc sulfide is an appealing candidate for photocatalysis of hydrogen production because of its: (i) ability to rapidly generate mobile photoexcited charge carriers [4]; (ii) high conduction band potential, which ensures fast electron transfer; and (iii) active sites for hydrogen evolution without the assistance of metal co-catalysts [5–7]. However, the performance of ZnS in photocatalysis has been restricted by its wide band gap (\sim 3.66 eV), which means that pure ZnS photocatalysts are only active under UV irradiation [7]. Suppressing charge recombination has also been a significant challenge [5,6].

Consequently, several attempts have been made to modify the light absorption behavior of ZnS. For example, it has been reported that 30% La-doped ZnS films have a band gap of 2.82 eV and give enhanced efficiency for photocatalytic dye degradation under visible light compared with undoped ZnS [8]. In addition, metal

E-mail address: j.hart@unsw.edu.au (J.N. Hart).

(Cu or Ni) doped ZnS prepared by a coprecipitation method has the ability to generate H₂ under visible-light irradiation [9,10]. However, maintaining charge balance when a dopant is introduced into the host lattice is difficult; this makes achieving high dopant concentrations challenging, and often only weak visible-light absorption is observed [10–14].

An alternative approach to doping for achieving visible-light activity may be defect engineering. While defects in semiconductors may act as recombination centers and hence decrease photocatalytic activity [15], they can also introduce new energy levels within the band gap that may produce visible-light activity, thus improving photocatalytic performance. For example, oxygen vacancies have been found to play an important role in TiO₂ [16,17] and Fe₂O₃ [18] photocatalysts that are active under visible light. It has been found that lattice sulfur vacancies in colloidal ZnS particles can produce trap states at a depth of 0.75 eV [19]. In addition, the inclusion of both shallow (e.g. lattice vacancies) and deep trap states (e.g. surface vacancies) can help to promote charge separation and suppress rapid electron-hole recombination [19-21], thus eliminating the second major shortcoming of ZnS photocatalysts. Careful defect engineering could therefore be exploited to enhance the overall photoelectrochemical properties of ZnS.

One way to control defect formation is by using a background gas during film growth by pulsed laser deposition (PLD). This has been reported for some oxide compounds, including indium tin oxide (ITO) [22] and zinc oxide (ZnO) [23]. For ITO film growth by PLD, the effect of various background gases (N₂, O₂, and Ne) was investigated. It was found that nitrogen gas promotes the formation of oxygen

^{*} Corresponding author.

vacancies, thus allowing highly conductive films to be synthesized by PLD at room temperature. For ZnO, vertically aligned nanowires have been grown by high-pressure-assisted PLD. The effects of oxidation as well as gas-phase collisions in the formation of nanowires were investigated using three different background gases: O₂, Ar, and O₂/ Ar mixture. PL spectra indicated that a high density of defects could be achieved.

In this paper, we report high photoelectrochemical activity of ZnS thin films under visible light, even though undoped ZnS should be active only at UV wavelengths. This is achieved through the purposeful introduction of defects in thin films deposited by PLD in a nitrogen atmosphere.

2. Experimental

2.1. Experimental method

ZnS thin films were grown on (001) Si substrates by PLD (KrF, λ =248 nm). The films were deposited with a substrate temperature of 500 °C under different N₂ background pressures, from vacuum $(10^{-6} \, \text{mTorr})$ to 100 mTorr of N₂. The laser fluence was fixed at 1.5 $\,\mathrm{J\,cm^{-2}}$. Throughout this paper, the labels ZnS-xx are used to refer to ZnS films deposited with different N₂ background pressures, where xx is the N₂ pressure, in mTorr, used during the film deposition. The film structure and cystallinity were characterized by Empyrean XRD (X'pert, Panalytical). The surface morphology of the films was studied by high resolution field emission SEM (FEI Nova NanoSEM 230). Photoluminescence spectra were acquired with a Renishaw inVia Raman Microscope using 325 nm laser wavelength. The photoelectrochemical measurements were conducted using an Autolab potentiostat (PGSTAT302N) from -1.0 V to 1.0 V in a three-electrode configuration with Pt as the counter electrode, Ag/AgCl as the reference electrode, and the ZnS film as the working electrode, 0.24 M Na₂S and 0.35 M Na₂SO₃ were used as the electrolyte solution. N₂ gas was bubbled through the electrolyte for 30 min prior to the measurements to remove any dissolved gases. The samples were irradiated with a 300 W Xe lamp (Oriel). For measurements under visible-light irradiation, a cutoff filter was used to remove UV wavelengths and obtain light only of wavelengths $\lambda \ge 435$ nm. Action spectra measurements were taken at 1.0 V bias in H₂SO₄ electrolyte solution using a Newport integrated monochromator to produce monochromatic wavelengths.

2.2. Computational method

Density functional theory (DFT) calculations were performed with the CRYSTAL09 code [24,25] using the B3LYP hybrid method [26,27]. Previously published basis sets were used, with the valence function parameters re-optimized for pure ZnS [28-30]. The Monkhorst-Pack grid for k-points sampling was set at a minimum of $8 \times 8 \times 8$ for the Brillouin zone; convergence with respect to the number of k-points was checked. Defective ZnS was simulated by removing/adding one Zn atom or S atom in a 64-atom supercell (a $2 \times 2 \times 2$ expansion of the conventional ZnS unit cell). The positions of the valence and conduction bands were aligned relative to the vacuum energy level by calculating the 1s orbital energies for atoms in the center of a ZnS slab with a vacuum gap between periodic images of the slab. The nonpolar (110) surface was used for the slab; the slab thickness was 20 atomic layers (\sim 36 Å, total of 40 atoms) and convergence with respect to the slab thickness was checked. A $24 \times 24 \times 1$ Monkhorst-Pack kpoint grid was used for the slab calculation. The 1s orbital energies for Zn and S atoms as far as possible from the defect in the defective cells were then adjusted to the values obtained for the ZnS slab and the same correction was applied to the valence and conduction band energies to give values relative to the vacuum energy. The valence and

conduction band energies obtained for defect-free ZnS by this method are in good agreement with previous reports [31].

3. Results and discussion

3.1. Structural and optical properties

The structural and optical characteristics of the ZnS thin films grown on silicon substrates by PLD under different N₂ background gas pressures, from vacuum to 100 mTorr, are shown in Fig. 1. The thickness of the film grown under vacuum is $\sim 2~\mu m$; the thickness decreases to $\sim 1~\mu m$ for the film grown under 100 mTorr N₂ pressure. The X-ray $\theta-2\theta$ pattern (Fig. 1(a)) for the ZnS film grown under vacuum has a peak at a d-spacing of 3.107 Å indicating that the ZnS is in the zinc blende phase. With increasing N₂ pressure, shoulder peaks start to appear at d-spacings of (3.107+0.182) Å and (3.107-0.122) Å, which indicate partial phase transformation of the ZnS to the wurtzite phase.

The photoluminescence (PL) spectra (Fig. 1(b)) show several peaks within the visible-light wavelength region. Peaks are observed at \sim 450, \sim 570, and \sim 760 nm, while no peaks are seen in the visible-light range in the PL spectrum of the bare silicon substrate. No PL emission at these wavelengths would be expected for bulk, defect-free ZnS, and we propose that these peaks are related to defects in the ZnS crystal structure, in agreement with previous reports [32,33]. For example, a PL peak at \sim 460 nm has been previously observed in zinc blende ZnS and attributed to the presence of zinc vacancies [19]. The intensity of the PL emission clearly increases as the N₂ pressure used during film deposition increases, particularly at the longest wavelengths; this may be attributed to an increase in the defect concentration.

TEM images of the ZnS films grown under vacuum and 100 mTorr N_2 pressure are shown in Fig. 1(c) and (d), respectively. The regular atomic arrangement of ZnS (Fig. 1(c)) with the marked d-spacings of 0.31 nm and 0.27 nm in the shell area correspond to the (1 1 1) and (0 0 2) lattice fringes of zinc blende ZnS, confirming the XRD results. In Fig. 1(d), the disorder of the atomic arrangement in the ZnS-100 sample is clearly visible, with local structural changes and variation in the atomic spacing, due to the presence of the N_2 gas during film deposition. This increased disorder in the structure deposited with the highest N_2 pressure is consistent with the higher PL emission.

In the XPS spectra, all samples show a Zn $2p_{3/2}$ peak at a binding energy of ~ 1022.2 eV and a S $2p_{3/2}$ peak at ~ 161.9 eV (Fig. 2), which are typical characteristics of ZnS [34]. As the background gas pressure used during film deposition increases, additional XPS peaks appear for both Zn and S at lower binding energies. This peak position for Zn is not consistent with ZnO [34]. As discussed later, and in agreement with both the PL spectra and the TEM images, it is likely that these peaks are due to defects in the ZnS structure. The Zn:S ratio determined by XPS (included in Supplementary material, Table S1) show that the films are Zn deficient, again indicating that the ZnS films are defective.

Peaks for oxygen were seen in the XPS spectra for all samples, with O 1s peaks at \sim 531.5 and \sim 533.2 eV, due to chemisorbed oxygen and adsorbed hydroxyl groups, respectively [34]. The XPS results indicated that the oxygen content of the samples was \sim 10 at% (Supplementary material, Table S1); there was no significant variation in oxygen content between the samples. It

¹ The UV-visible spectra were measured, but they are dominated by interference effects at visible-light wavelengths (Supplementary material, Fig. S1), making interpretation difficult. For this reason, we have only presented PL spectra here. We also discuss below the PEC measurement of action spectra, which are included in Supplementary material; these provide similar information regarding wavelength-dependent activity to UV-visible spectra.

Download English Version:

https://daneshyari.com/en/article/6534710

Download Persian Version:

https://daneshyari.com/article/6534710

<u>Daneshyari.com</u>